Towards Generalizable Classification of Partial Discharges in Gas-Insulated HVDC Systems Using Neural Networks: Protrusions and Particles

Steffen Seitz, Thomas Götz, Christopher Lindenberg, Ronald Tetzlaff, *Senior Member, IEEE*, and Stephan Schlegel

***Abstract*—Undetected partial discharges (PDs) are a safety critical issue in high voltage (HV) gas-insulated systems (GIS). While the diagnosis of PDs under AC voltage is well-established, the analysis of PDs under DC voltage remains an active research field. A key focus of these investigations is the classification of different PD sources to enable subsequent sophisticated analysis. In this paper, we present an analysis of a 1D-CNN-based approach for classifying laboratory PD signals caused by metallic protrusions and conductive particles on the insulator of HVDC GIS, under both negative and positive potentials. Most notably, our study demonstrates that this type of neural network, regardless of the training order, can generalize learnings to operating voltage multiples that it has not previously encountered. We evaluate this generalization performance under the presence of additional white Gaussian noise and investigate the influence of excluding the amplitude-related information in the signal. Further, we compare the network's performance when using input signals in both the time and frequency domain.**

***Index Terms*—Fault diagnosis, HVDC, partial discharge, neural networks, machine learning.**

I. Introduction

THE increasing integration of renewable energy sources into the existing high-voltage grid requires the use of high-voltage direct current (HVDC) systems. This technology is superior to conventional AC technology for transmitting large amounts of power over long distances because of lower losses, and the elimination of reactive power. Apart from high efficiency, the compact installation of high-voltage equipment is also a critical consideration. Both requirements, high-efficiency power transmission and space-saving installation, are met by gas-insulated systems (GIS), which have been developed for use in transmission systems under AC voltage stress since the 1960 s.

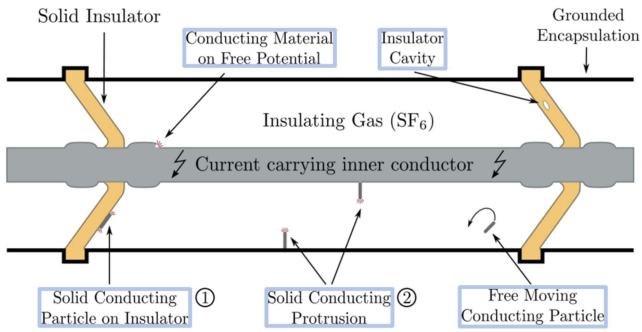

Fig. 1. Schematic representation of a HVDC gas-insulated system and related typical partial discharges generating defects. The presented work aims to classificate UHF PD signals caused by particle- ① and protrusion-based ② defects.

A crucial aspect of ensuring fault-free operation in HVDC GIS is the automatic classification of PD-generating defects based on measurement recordings [1]. Fig. 1 illustrates a typical HVDC GIS and its common sources of PDs. This includes solid metallic particles on the insulation, on free potential or freely moving in the insulating gas, and conducting protrusions on the encapsulation or conductor [2]. In contrast to conventional AC GIS, the number of these devices in operation under DC stress is rather low. Thus, the measurement [3], classification [4], and physical interpretation [5] of DC PDs continue to be active areas of research.

Recently, studies investigating PD development in HVDC GIS indicate that the physical processes responsible for PD formation are the same as compared to those observed under AC voltage stress [6]. However, due to the constant electric field, continuous directed movement of charge carriers and the generation of space and surface charges, the behavior of DC PD events, such as amplitude and repetition rate, differs significantly from AC PDs [2]. As a result, the methods and findings related to AC PD classification cannot be directly applied to HVDC GIS. For example, the well-established AC GIS PD detection method, which relies on measurements in the ultra-high frequency (UHF) range and human expert evaluation of phase-resolved partial

Manuscript received 14 July 2023; revised 26 November 2023 and 22 January 2024; accepted 11 February 2024. Date of publication 26 February 2024; date of current version 23 May 2024. This work was supported in part by the German Research Foundation DFG, under Project 379542208 and in part by the German Federal Ministry of Economic Affairs and Climate Action BMWK under Grant KK5056101KA0. Paper no. TPWRD-00995-2023. *(Corresponding author: Steffen Seitz.)*

Steffen Seitz, Christopher Lindenberg, and Ronald Tetzlaff are with the Department of Electrical and Computer Engineering, Technische Universität Dresden, 01062 Dresden, Germany (e-mail: steffen.seitz@tu-dresden.de).

Thomas Götz and Stephan Schlegel are with Department Electrical Power Systems and High Voltage Engineering, Technische Universität Dresden, 01062 Dresden, Germany.

Color versions of one or more figures in this article are available at https://doi.org/10.1109/TPWRD.2024.3369872.

Digital Object Identifier 10.1109/TPWRD.2024.3369872

discharge (PRPD) plots [7], [8], is not suitable for distinguishing DC PD source signals due to the lack of necessary phase information. Consequently, the development and testing of novel DC-specific PD classification methods are essential for ensuring the safety of HVDC GIS.

The most advanced technique for evaluating and identifying PDs under DC voltage stress is pulse sequence analysis (PSA) based on the evaluation of time-resolved partial discharge (TRPD) plots. This method involves the assessment of patterns by human experts [9]. Hence, the amplitude and time information of individual PD events in the UHF signal are leveraged to identify the defect corresponding to the signal [10]. However, this approach relies on time-consuming human judgment and it is limited to scenarios with a single PD source. In situations where multiple sources are active, the PD signals overlap, hindering clear identification and necessitating the use of complex techniques for source separation [11], [12].

To achieve an automatic PD signal classification, Schober and Schichler [13] proposed a machine learning-based approach for PD measurements from GIS under DC. Their novel approach employed Support Vector Machines and neural networks to assess PSA features derived from UHF measurements. Despite its promising results, this method inherits the limitations associated with hand-crafted PSA features such as challenges in classifying signals of multiple active PD sources.

Neural networks, such as multi-layer perceptrons (MLP) or convolutional neural networks (CNN), have been used to classify PDs under AC utilizing TRPD [14], [15], [16] and PRPD [17], [18], [19] features with remarkable results. Most notably when directly applied to time-domain measurements, they have demonstrated potential in effectively distinguishing multiple active signal sources in GIS under AC [20] and similar domains [21]. Hence, if applicable to DC GIS PD classification, they could potentially obviate the necessity for PSA and source separation techniques. Therefore, Beura et al. [22] introduced the first study of CNN for feature extraction from UHF time-domain measurements under DC. Their study demonstrated comparable results to the pre-existing PSA methods [13]. However, there are still several critical questions vital for the practical application of this method that remain unanswered.

First, as already illustrated in Fig. 1, DC PDs in GIS originate from multiple defect types. PDs generated by particles and protrusions on the insulator surface a are particularly significant [10]. However, the existing literature does not provide sufficient evidence regarding the capability to classify these specific fault types. Moreover, there is a lack of information regarding the classification accuracy of neural network models at both, negative and positive polarities of the inception voltage. However, this information is crucial for a risk assessment of the asset and a successful transfer of the laboratory experiment results to on-site installations [2].

In addition, previous studies under AC stress have demonstrated that utilizing fast Fourier transform (FFT) coefficients extracted from UHF signals as training data yields improved PD classification results under AC [23]. Therefore, it would be advantageous to explore the transferability of these AC findings to the DC PD classification domain.

Furthermore, all typical defects of HVDC GIS can experience stress from various multiples of the inception voltage U_i. These individual voltages lead to slightly different discharge patterns [2]. However, the specific U_i at the on-site GIS is not known in practice and creating a suitable amount of data for every combination of the defect type and U_i multiple is impractical for experts. In addition, during site-acceptance tests, it is common practice to intentionally vary the DC voltage across a broad range, ranging from 0 kV to multiples of the nominal voltage. Depending on the respective project this voltage is at least 1.2 times the nominal voltage. Thus, it is essential to investigate the ability of a PD classification model to generalize to measurements based on unseen U_i multiples. This investigation ensures that the results obtained can be directly applicable to on-site GIS and site-acceptance tests.

Another challenge in HVDC GIS arises from the amplitude of UHF PD signals, which is influenced by free-space path loss, particularly when the signal has to cross barrier insulators. Thus, the amplitude is proportional to the distance between the defect location and the sensor. As this distance varies in applications outside laboratory tests, it might be advantageous to study the influence of amplitude-related information on the model performance by applying different normalization methods. In summary, this study contributes to the HVDC GIS PD classification in three significant aspects:

- First, we provide the missing evidence that a 1D-CNN-based architecture can effectively classify DC PD time-domain UHF signals originating from particles on an insulator and fixed metallic protrusions at both, negative and positive DC voltage stress.
- Second, we present the first investigation of an HVDC PD classification model in terms of its ability to classify measurements obtained at multiples of the inception voltage U_i that have never been included in the model training. Hence, we aim to estimate the model's ability to generalize from laboratory data to measurements of on-site installations under unknown DC voltage stress levels.
- Third, we analyze the impact of removing the amplitude-related signal content on the PD classification model by investigating different normalization methodologies.

II. Experimental Setup & Methods

This study is conducted using UHF DC-PD signals measured under DC voltage stress, as documented in Götz [2] and Götz et al. [6]. The measurements were performed in a gas-insulated test setup shown in Fig. 2 (top). The model electrode arrays are installed inside a test vessel to simulate the typical behaviour of the defects. The tests were performed using sulfur-hexafluoride (SF_6) as the insulation gas at an absolute pressure of 0.5 MPa. In the protrusion arrangement (Fig. 2; bottom, right), the metallic protruding needle has a length of 5 mm and the needle tip is installed at a distance of 55 mm from the opposing high-voltage electrode.

To simulate PD at the gas-solid interface (Fig. 2; bottom, left), a 13 mm needle is placed on the surface of an epoxy insulator, typically used in gas-insulated systems. The distance

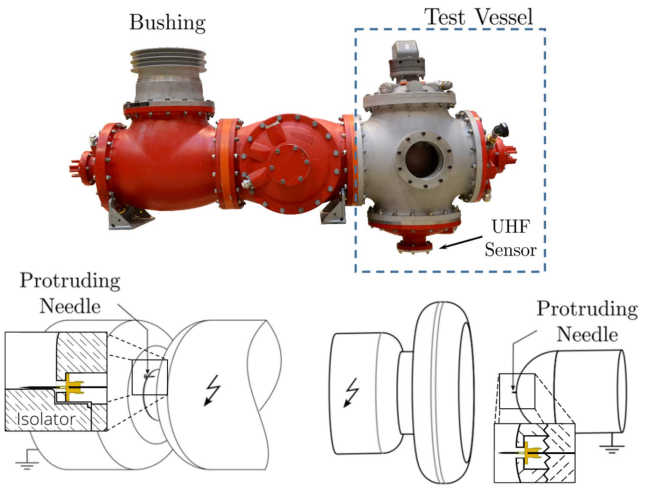

Fig. 2. Picture of the experimental setup (top) and three-dimensional schematics of the electrode arrangements used for the emulation of DC-PD at the gas-solid interface (bottom, left) and at a fixed metallic protrusion (bottom, right) [2].

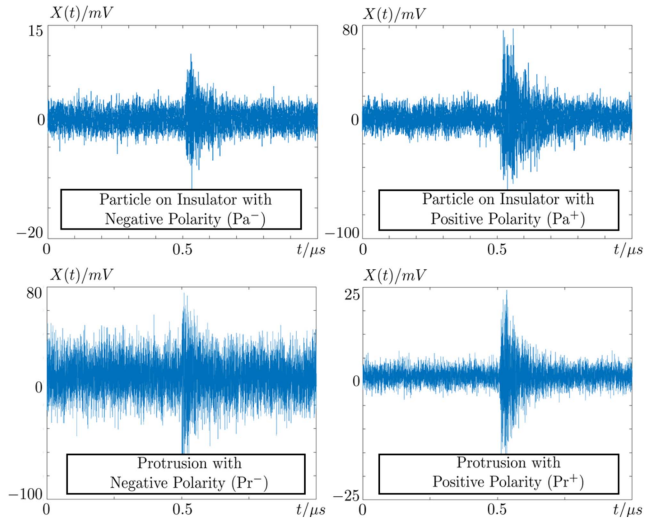

Fig. 3. Time-domain signal examples of the considered defects. Each PD measurement is based on either particles at the gas-solid interface (Pa^-, Pa^+) or protrusions (Pr^-, Pr^+) at negative and positive potential of the needle electrode.

between the needle tip and the opposing high-voltage electrode is 26.7 mm. The high DC voltage with positive and negative polarity up to voltages of 250 kV and a ripple content δU of below 0.1% is applied from zero at a rate of 0.5 kV/s via the air-SF_6 bushing installed in the centre of the test vessel. The specified voltage levels were applied over several minutes before recording the UHF signal. The PD signal is then detected using a UHF sensor [24] installed in the test vessel. A 30 dB amplifier is used to increase the signal-to-noise ratio (SNR). The PD signals are sampled at 10 GS/s using a Teledyne LeCroy WavePro 735 ZiA digital oscilloscope. Some example recordings are depicted in Fig. 3.

Due to the physical nature of the discharge process, each partial discharge impulse has a total length of several ten picoseconds, regardless of the type of applied voltage (AC or DC) [6]. The time difference between subsequent impulses, and therefore the repetition rate, is strongly depending on the applied voltage. It is in the range between a few microseconds up to several minutes [6]. Due to the low ripple content in the applied DC voltage, the discharges do not show a frequency dependent repetition rate, while under AC this depends on the power frequency. It should be noted that in Fig. 3 we chose to plot only 'similar' single impulses for brevity. The measurements in our dataset include more than just single impulses and are affected by various noise levels.

Each i-th measurement $M_j = \{s_{j,1}, \ldots, s_{j,u}, \ldots, s_{j,l_s}\}, j \in \{1, \ldots, N\}$ has a length of $l_s = 20002$ individual samples $s_{j,u} | s \in \mathbb{R}$, sampled at time step u. The resulting data set contains a total of $N = 33000$ individual PD measurements taken at different multiples of the inception voltage U_i. A so-called source class label is assigned to each M_j based on the defect type, the polarity of the needle and the U_i multiple. The number of source class measurements is shown in Table I.

This U_i-information is only utilized to investigate the generalization capability of the model (Section III-B). In the classification task the model discards this information and learns to predict the so-called output class labels (Fig. 3) based on the given source class measurement. Thus, the output class labels are based on the defect type and needle polarity.

TABLE I
NUMBER OF AVAILABLE MEASUREMENTS M_j OF EACH SOURCE CLASS IN THE DATASET OF [2]

		Negative Polarity			Positive Polarity		
Particle		$Pa^-_{1\cdot U_i}$	$Pa^-_{1.5\cdot U_i}$	$Pa^-_{3\cdot U_i}$	$Pa^+_{1\cdot U_i}$	$Pa^+_{1.25\cdot U_i}$	$Pa^+_{1.5\cdot U_i}$
		3500	3500	3500	3500	3500	3500
Protrusion		$Pr^-_{2\cdot U_i}$	$Pr^-_{3\cdot U_i}$	-	$Pr^+_{2\cdot U_i}$	-	-
		4000	4000	-	4000	-	-

In each of our experiments, the data is randomly drawn from these recorded measurements and divided into a training and a test set by allocating 80% of the measurements of each class to the training set D_{train} and the remaining 20% to the test set D_{test} which are normalized using three different methods.

A. Normalization Methods

The objective of data normalization or min-max scaling is to standardize features to a consistent scale. This typically leads to improved performance and training stability of the model. However, dependent on the choice of the method, its application may affect the information contained in the signal. Normalization can be applied in three different ways:

1) Trainset Normalization (Tr): In trainset normalization, every sample in each measurement M_j within D_{train} and D_{test} is normalized between -1 and $+1$ according to:

$$\bar{s}_{j,u} = \frac{s_{j,u} - \text{Min}(D_{\text{train}})}{\text{Max}(D_{\text{train}}) - \text{Min}(D_{\text{train}})}. \quad (1)$$

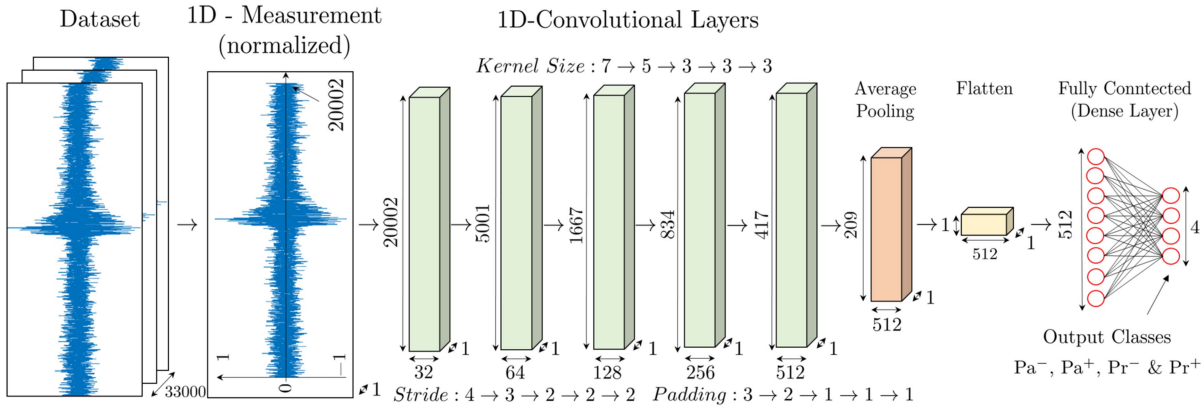

Fig. 4. Proposed model consists of five consecutive 1D-CNN layers with ReLU activation, followed by an average pooling- and a flatten layer. The features are fed into a fully connected multi-layer perceptron. This network has 512 ReLU neurons in the input layer and four output neurons with a softmax activation to assign one of the output classes (Pa$^-$, Pa$^+$, Pr$^-$, Pr$^+$).

Min/Max$(\cdot)$ are operations that return the min-/maximum value of any individual measurement within the dataset. As shown in (1), trainset normalization scales each sample in each measurement with respect to the maximum and minimum sample value of all individual measurements across all classes in the dataset. Thus, this method preserves the amplitude information for each measurement in the dataset. However, due to the previously stated free-space path loss problem, it might be advantageous to generally exclude amplitude-related information during model training.

2) Class Normalization (Cl): Class normalization scales each sample within a measurement relative to the maximum and minimum sample values of all measurements belonging to the corresponding source class from Table I. In this method, the amplitude-related information is preserved within samples of one class, while it is hidden between measurements of different classes.

3) Measurement Normalization (Me): In measurement normalization, each sample in a measurement M_j is scaled based on the maximum and minimum sample values within that specific measurement period in the dataset. In this case, the model can no longer rely on amplitude-related features to classify different samples of class in the dataset.

B. Classification Model

In our experiments, the normalized UHF amplitude signal measurements and their respective FFT coefficients are separately used to train the neural networks-based model as depicted in Fig. 4. These networks use sample measurements and their assigned output class labels in D_{train} to learn their weighting and bias parameters and ultimately predict the correct output class label.

The architecture in our work is based on 1D-convolutional [25] and perceptron layers [26]. We tested different numbers and arrangements of these layer types in conjunction with different activation functions such as ReLU, Sigmoid, and Tanh to achieve an improved classification result. For brevity, only the final model structure is given. This structure and the corresponding activation functions were empirically determined with respect to maximizing classification performance.

In the final architecture, the 1D-convolutional layers perform sequential, discrete convolutions between a filter kernel and the data. The extracted features are processed by a ReLU activation function after each layer followed by an average pooling layer and a flattening layer. The data is further processed by the perceptron layer with 512 neurons and a ReLU activation function, which maps the extracted information to the output classes depicted in Fig. 3.

The model parameter adjustment is performed using a NVIDIA A100 and the PyTorch library. The optimal parameter set is determined by optimizing a cross-entropy loss using ADAM optimization [27]. The initial learning rate of 0.0001 and a batch size of 64 were determined through a random search. In each of our experiments, the network is initialized with 15 different weight initialization seeds to account for the effects of a non-optimal start to the optimization process. The number of individual seeds was chosen to represent a reasonable trade-off between the statistical robustness of the result and the computational time of the model. The performance of each trained model is evaluated using unseen data from D_{test}. In addition, similar to k-fold cross-validation, a different set of measurements from the limited experimental data is randomly assigned to D_{train} and D_{test} in each of the 15 training and testing procedures. The obtained classification results are averaged to determine a more reliable true positive rate A of the proposed architecture for each defect class. Similarly, the true negative, false negative, and false positive rates of the model are determined for all other output classes.

III. Experiments & Results

A. Time- and Frequency-Domain Classification Results

In this section, we analyze the capability of the proposed architecture to classify unseen measurements of PD generated by a fixed protrusion or a particle adhering to the gas-solid interface. To accomplish this, we utilize UHF signals measured in either the time-domain or frequency-domain at a specific U_{i}

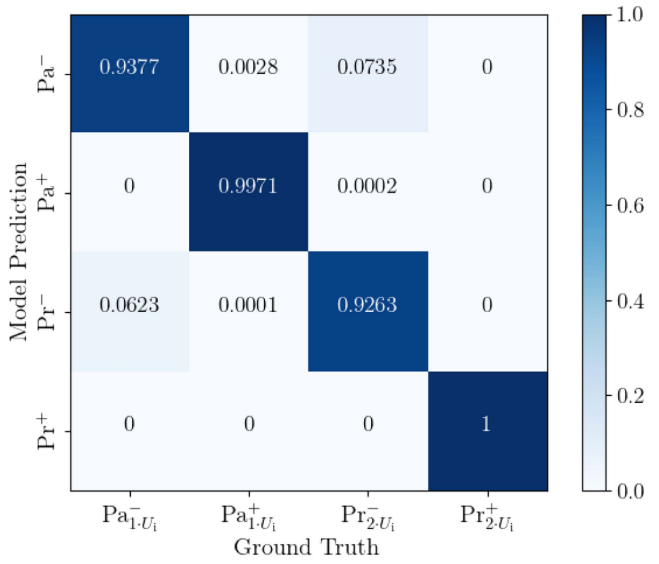

Fig. 5. Model confusion matrix ($\bar{A}_{\text{trainset}} = 0.9653$) obtained by utilizing $\text{Pa}^-_{1\cdot U_\text{i}}$, $\text{Pa}^+_{1\cdot U_\text{i}}$, $\text{Pr}^-_{2\cdot U_\text{i}}$ and $\text{Pr}^+_{2\cdot U_\text{i}}$ time-domain measurements, preprocessed by trainset normalization.

multiple for each output class. In this initial experiment, the baseline dataset D comprises measurements of $\text{Pa}^-_{1\cdot U_\text{i}}$, $\text{Pa}^+_{1\cdot U_\text{i}}$, $\text{Pr}^-_{2\cdot U_\text{i}}$, and $\text{Pr}^+_{2\cdot U_\text{i}}$, which are then divided into D_train and D_test. However, while it would be beneficial to classify the output class based on data measured at the same constant multiple of U_i, for technical reasons the available dataset only contained an unbalanced measurement distribution [2]. As a result, there is an unequal distribution of measurements recorded at the same U_i multiples for each output class, as shown in Table I.

Fig. 5 illustrates the confusion matrix of the experiment involving the proposed output classes $\text{Pa}^-_{1\cdot U_\text{i}}$, $\text{Pa}^+_{1\cdot U_\text{i}}$, $\text{Pr}^-_{2\cdot U_\text{i}}$ and $\text{Pr}^+_{2\cdot U_\text{i}}$. The model achieves a near-perfect true positive rate A for UHF signals resulting from positive particle (Pa^+) or positive protrusion (Pr^+) defects. For the remaining two output classes, the model obtains only a slightly worse result. In particular, it exhibits a nearly symmetrical confusion between measurements associated with negative particles (Pa^-) and negative protrusions (Pr^-). As mentioned in Section II-B, the model in this experiment was trained separately with 15 different weight initialization seeds. Thus, the presented classification rates of each class in the confusion matrix are the average across all individual runs. The overall performance of the architecture is represented by the average true positive rate $\bar{A}$. It is determined by averaging the individual true positives of all output classes in the confusion matrix. In Fig. 5, these values are indicated by the diagonal elements of the matrix, representing the true positive rate of correctly classified PD samples for each class, while the non-diagonal elements represent the false positive and true negative rates when comparing the predicted class against the ground truth. It is important to note that all the accuracy results presented in this study are likely applicable to different sensor positions and distances within our linear GIS test segment [28]. However, it's crucial to recognize that this may not hold true for complex GIS structures, such as L-shapes,

TABLE II
AVERAGE TRUE POSITIVE CLASSIFICATION RATES $\bar{A}$ FOR DIFFERENT NORMALIZATION STRATEGIES AND INPUT DATATYPE

Input Datatype	Normalization Method		
	Measurement (Me)	Class (Cl)	Trainset (Tr)
Time-Domain (TD)	**0.9977**	0.9932	0.9653
Freq.-Domain (FFT)	**0.9983**	0.9975	0.8048

where the frequency selective transfer function between the PD source and the sensor significantly influences the signal characteristics [29].

As summarized in Table II, the trained model achieves an $\bar{A}_\text{Tr} = 0.9653$ on the trainset normalized measurements in D_test. The performance on time-domain test data is generally better if the amplitude information is at least partially- ($\bar{A}_{\text{Cl, TD}} = 0.9932$), or completely- ($\bar{A}_{\text{Me, TD}} = 0.9977$) hidden after normalization. If the time-domain input data is converted to the frequency-domain instead, the classification rate based on the trainset normalized FFT coefficients only achieves an average of $\bar{A}_{\text{Tr, FFT}} = 0.8048$. Thus, if trainset normalization is selected and the model generalization to unseen U_i multiples is not required, time-domain data should be used to train the classifier. Analog to the time-domain signal, the FFT-based true positive rate is higher for class- and measurement normalization. Classifying PDs from the FFT coefficiants of the UHF signal resulted in the highest classification performance in our experiments, with $\bar{A}_{\text{Me, FFT}} = 0.9983$. Therefore, the minor difference in performance compared to using the time-domain data hardly justifies the computational cost of converting every measurement to the frequency-domain. Thus, the following experiment relies solely on the time-domain data.

B. *Generalization to an Unseen Multiple of U_i)*

As previously mentioned in Section I, it is important to examine PD classification models in terms of their generalization to measurements of defects recorded at unknown multiples of the GIS inception voltage (U_i). Therefore, each PD measurement is assigned a source class based on the defect type and the inception voltage determined at the time of recording. Note that the exact value of U_i does not need to be further specified, since the approach of this work is centered around the idea of using laboratory data at specific U_i multiples to train a model that generalizes to data from unknown U_i multiples at the on-site GIS.

In the first part of our experiment, we evaluate the generalization performance. Hence, we pre-train our model based on the data of the same source classes used in Section III-A ($\text{Pa}^-_{1\cdot U_\text{i}}$, $\text{Pa}^+_{1\cdot U_\text{i}}$, $\text{Pr}^-_{2\cdot U_\text{i}}$ and $\text{Pr}^+_{2\cdot U_\text{i}}$), to create a baseline for our further studies. Note, that analog to the previous experiment, any measurement is normalized by either trainset-, class-, or measurement normalization. After the training process, the generalization performance of the baseline model is assessed by monitoring the model generalization rate G, which is equal to the true positive rate of the model on the untrained $\text{Pa}^+_{1.5\cdot U_\text{i}}$ measurements in the test set, i.e. $G := A(\text{Pa}^+_{1.5\cdot U_\text{i}})$. Note, that the data of

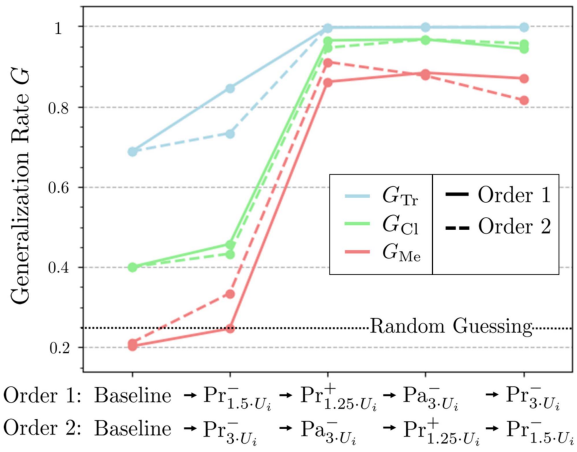

Fig. 6. Model generalization rate G on the untrained U_i multiplier $\mathrm{Pa}^+_{1.5\cdot U_\mathrm{i}}$ when additional data from a specific previously withheld source classes is included in the D_train. The issue is investigated for trainset (Tr), class (Cl), and measurement (Me) normalization and two different sequential training orders.

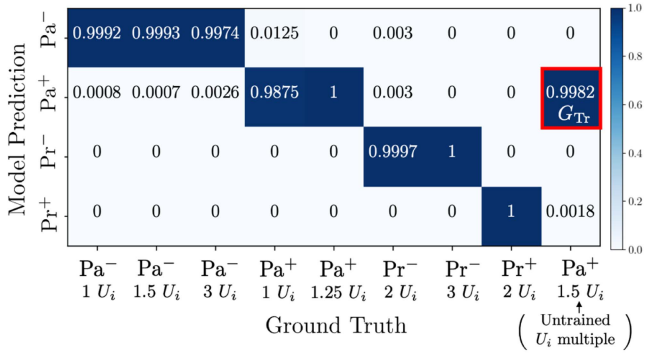

Fig. 7. Confusion matrix and generalization rate G_Tr (red) of the proposed model. The network was trained using the full trainset-normalized measurements of all available classes from Table I (except $\mathrm{Pa}^+_{1.5\cdot U_\mathrm{i}}$), using the train sequence of order 1.

$\mathrm{Pa}^+_{1.5\cdot U_\mathrm{i}}$ is explicitly excluded from the training set in any of the further experiments. Therefore, the described measurements are used only at inference time to test the model's generalization to an unseen source class. In this setting, the model can only rely on the knowledge learned from the source class data available in D_train to classify any of the $\mathrm{Pa}^+_{1.5\cdot U_\mathrm{i}}$ measurements in D_test.

When trainset normalization (Tr) is used to normalize the baseline dataset (Base), the model achieved a generalization rate of $G_{\mathrm{Tr,Base}} = 0.6801$. With class normalization (Cl), the model achieved a significantly lower result of $G_{\mathrm{Cl,Base}} = 0.4010$, while with measurement normalization, the generalization rate of $G_{\mathrm{Me,Base}} = 0.2085$ did not outperform a random classifier in classifying our four output classes ($G_\mathrm{r} = 0.25$). A possible explanation could be the lack of amplitude-related information after data preprocessing with these normalization methods. To investigate this issue further, we refine our basic model by gradually adding measurement data from a previously withheld source class to the trainset D_train. The extended training set is used to train the model from scratch. In parallel, the generalization rate of the model is determined after each addition, analogous to the baseline experiment. The sequential training was performed for two different consecutive sequence orders ("Order 1" and "Order 2") to rule out any effects of adding a single record to D_train.

The results of this experiment shown in Fig. 6 indicate that the model achieves a generalization rate that is reliably above the baseline results, regardless of the normalization type and sequential ordering, after data from the first additional U_i multiple is added to the baseline dataset. After training the model with data from all available source classes in Table I (except for the $\mathrm{Pa}^+_{1.5\cdot U_\mathrm{i}}$ data), a generalization performance is achieved that far exceeds random guessing. Analog to training with a single additional source class, this result is independent of the type of normalization and the sequential order. In contrast to the previous experiment from Table II, trainset normalization performs best in the generalization setting. The highest generalization rate with trainset normalization was achieved after training with order 1 (O1), resulting in $G_{\mathrm{Tr,\,O1}} = 0.9982$. In comparison, the highest generalization rate of class normalization at the end of order 2 (O2) achieved $G_{\mathrm{Cl,\,O2}} = 0.9578$. The highest measurement normalization based approach only achieves $G_{\mathrm{Me,\,O1}} = 0.8672$ at the end of order 1. As for the baseline dataset, a possible explanation could be the lack of amplitude-related information after data preprocessing with these normalization methods. In practice, the model is expected to generalize from laboratory measurements to data of a monitored GIS with an unknown U_i multiple. Therefore, assuming negligible effects of the frequency selective free-space path loss on the classifier result for linear GIS segments under DC, similiar to the findings under AC from Li et al. [28], it is recommended to select normalization methods that preserve the amplitude information in the data.

Similar to Section III-A, it is crucial to evaluate model performance concerning the remaining source class measurements from Table I while assessing generalization on the withheld $\mathrm{Pa}^+_{1.5\cdot U_\mathrm{i}}$ data. When measurements of all source classes from Table I (exept $\mathrm{Pa}^+_{1.5\cdot U_\mathrm{i}}$) are included in D_train, the model classifies almost all test set measurements correctly. This is illustrated by the confusion matrix in Fig. 7.

For the sake of brevity, all combinations of normalization methods and training routines are not shown, as they achieved comparable results. In the depicted configuration, the average true positive rate over the available classes in the training set is $\bar{A}_{\mathrm{Tr,\,O1}} = 0.9979$. When this score is averaged with the associated generalization rate ($G_{\mathrm{Tr,\,O1}} = 0.9982$), the model attains an average final true positive rate of $\tilde{A}_{\mathrm{Tr,\,O1}} = 0.9977$ for all measurements across all classes in our experiment. This clear separability of the measurements indicates, that the respective defect signals change significantly when recorded at different voltages.

To evaluate the influence of noise on the generalization rate, in Fig. 8, we superimposed the trainset normalised PD test signals with white Gausian noise. To generate the depicted boxplot, we conducted 15 separate trials with different random noise initializations for each specific SNR level.

The results suggest that even when significant additional noise is introduced, such as at an SNR of 6, the network maintains

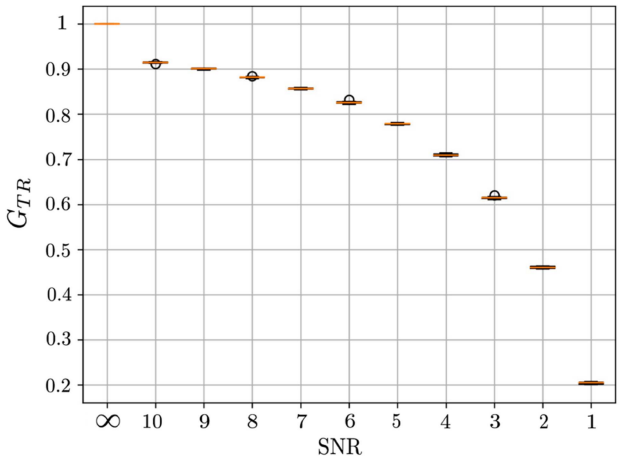

Fig. 8. Boxplot of the generalization rate G_{Tr} for PD signals superimposed with Gaussian noise as a function of the SNR.

classification accuracies above 80%, which would probably be sufficient for practical implementation.

C. Comparison to Other Methods

Comparing our results to the existing DC PD classification literature presents certain challenges. The study of Schober and Schichler [13] previously studied Pr and Pa classification, however their PSA-based method did not report individual classification rates for these PD types and did not evaluate different polarities as well as the generalization to unknown voltage levels. In addition, the number of measurements available for each class is very limited, making any comparative analysis on their average model accuracy even more difficult. The study of Beura et al. [22] reported individual performances for the Pr detection task. Our chosen CNN-based architecture achieves an 1.29% higher average performance than their model but, in constrast, for both possible needle polarities. They also did not evaluate any Pa-PDs as well as the generalizability of their model to other voltage and noise levels as their primary focus was to investigate the distinguishability of UHF PD signals in GIS without relying on PSA. While it is challenging to directly compare the results of our studied model to the existing literature on DC PD classification, our average results align with findings for CNNs under AC conditions [17], [19], [25].

It should be noted, that neither our study nor the study of Beura et al. [22] had a access to data of all possible PD types in DC GIS (see Fig. 1) since creating such a comprehensive GIS setup in a laboratory environment is both financially and temporally demanding. Therefore, the possibility of aliasing in CNN models may still exist when trained using comprehensive data. However, our results warrant such further testing of CNN methods with comprehensive on-site data. To conclude, our contributions to the field are summarized in Table III.

TABLE III
COMPARISON OF THE PRESENTED WORK TO RELATED NON-PSA-BASED PD CLASSIFICATION APPROACHES IN HVDC GIS

Category	**Our work**	[22]	[13]
Pr classification accuracy:	**99.99%**	98.23%	not reported
Pa classification accuracy:	**99.67%**	not investigated (n.i.)	not reported
Average per class test set size:	733	461	83
No PSA features required:	✓	✓	✗
Defect polarity studied on:	protrusion & solid particle on insulator	particle on free potential	n.i.
Normalization influence	✓	n.i.	n.i.
Generalization to U_{i} multiples:	✓	n.i.	n.i.
Noise influence:	✓	n.i.	n.i.

IV. Conclusion & Outlook

In this paper, we evaluate the performance of a neural network-based method to classify UHF measurements of DC partial discharges (PDs) generated by conductive protrusions and particles on an insulator at both negative and positive polarity, as well as generalization to different inception voltages. Our study extends the literature on HVDC GIS PD classification in multiple aspects:

- First, we report the first 1D-CNN-based model capable of classifying UHF signals originating from particles adhering to the gas-solid interface (insulators) and protrusions at different polarities. During our experiments, the use of frequency-domain signals achieved only a negligible average performance advantage compared to the UHF time-domain signal classification model result.
- Second, we are the first to investigate the ability of a neural network PD classification model to generalize to measurements recorded under unknown DC voltage stress levels. Regardless of the training order, the model correctly classifies 99.87% of the U_{i} multiple signals not included in the train set as well as 99.77% of all available PD test set measurements. Even in the presence of noise, the network achieved a result sufficient enough to warrant further testing of our methods with on-site data.
- Third, we analyzed the effect of excluding the amplitude-related signal content on the performance of a PD classification model in HVDC GIS through using sample-, class- and training set normalization. Our results indicate that even when using data with at least partially eliminated amplitude information, it is still possible to train effective models. These models suprisingly exhibited slightly superior performance classifying PD signals, although it is worth noting that models trained with amplitude-preserved data outperform on the generalization task.

In future work, a comprehensive model should be trained to classify measurements of all possible PD types in HVDC GIS

simultaneously, such as insulator cavities, free-moving particles, and material on free potential. We also suggest considering different electrode geometries and spacing to enhance the methodology. Furthermore, it would be important to study the influence of the frequency selective transfer function between the sensor and the defect location, as previously conducted in research under AC conditions. This investigation would contribute to the practical applicability of the method in real-world HVDC GIS scenarios.

ACKNOWLEDGMENT

The authors acknowledge the computing time through the ZIH at TU Dresden and the valuable feedback from Thomas Linde and Carsten Knoll.

REFERENCES

[1] N. Davies and D. Jones, "Testing distribution switchgear for partial discharge in the laboratory and the field," in *Proc. Conf. Rec. IEEE Int. Symp. Elect. Insul.*, 2008, pp. 716–719.

[2] T. Götz, "Partial discharge behaviour of gas-solid insulation systems under DC voltage stress," Technical Univ. Dresden, 2022. [Online]. Available: https://tud.qucosa.de/landing-page/?tx_dlf[id]=https%3A%2F%2Ftud.qucosa.de%2Fapi%2Fqucosa%253A80136%2Fmets

[3] A. Abbasi, J. Castellon, A. Cavallini, F. Esterl, and T. Götz, "Progress on partial discharge detection under DC voltage stress," in *Proc. CIGRE Joint Colloq. - SCA2/SCB2/SCD1*, 2019.

[4] A. Pirker and U. Schichler, "Partial discharges at DC voltage - measurement and pattern recognition," in *Proc. Int. Conf. Condition Monit. Diagnosis*, 2016, pp. 287–290.

[5] A. Mor et al., "Promotion: Progress on meshed HVDC offshore transmission network - report on diagnostic analysis and condition assessment (D15.5)." [Online]. Available: https://cordis.europa.eu/project/id/691714

[6] T. Götz, H. Kirchner, and K. Backhaus, "Partial discharge behaviour of a protrusion in gas-insulated systems under DC voltage stress," *Energies*, vol. 13, no. 12, 2020, Art. no. 3102.

[7] N. Achatz, J. Gorablenkow, U. Schichler, B. Hampton, and J. Pearson, "Features and benefits of UHF partial discharge monitoring systems for GIS," in *Proc. Int. Symp. Elect. Insulating Mater.*, 2005, pp. 722–725.

[8] T. Hoshino, H. Koyama, S. Maruyama, and M. Hanai, "Comparison of sensitivity between UHF method and IEC 60270 for onsite calibration in various GIS," *IEEE Trans. Power Del.*, vol. 21, no. 4, pp. 1948–1953, Oct. 2006.

[9] A. Pirker and U. Schichler, "Partial discharge measurement at DC voltage - Evaluation and characterization by NoDi* pattern," *IEEE Trans. Dielectrics Elect. Insul.*, vol. 25, no. 3, pp. 883–891, Jun. 2018.

[10] A. Pirker and U. Schichler, "Partial discharges at DC voltage - measurement and pattern recognition," in *Proc. Int. Conf. Condition Monit. Diagnosis*, Xi'an, China, 2016.

[11] B. Hochbrückner et al., "Digital filtering methods for interferences on partial discharges under DC voltage," in *Proc. 21st Int. Symp. High Voltage Eng.*, 2020, pp. 560–571.

[12] B. Hochbrückner, M. Spiertz, M. H. Zink, A. Küchler, and K. Backhaus, "Comparison of algorithms for clustering of partial discharge signals under DC voltage," in *Proc. 2nd Int. Conf. High Voltage Eng. Power Syst.*, 2019, pp. 041–046.

[13] B. Schober and U. Schichler, "HVDC GIS/GIL - machine learning algorithms for online PD classification at DC voltage," in *Proc. 9th Int. Conf. Condition Monit. Diagnosis*, 2022, pp. 225–230.

[14] L. Li, J. Tang, and Y. Liu, "Partial discharge recognition in gas insulated switchgear based on multi-information fusion," *IEEE Trans. Dielectrics Elect. Insul.*, vol. 22, no. 2, pp. 1080–1087, Apr. 2015.

[15] M. A. Khan, J. Choo, and Y.-H. Kim, "End-to-end partial discharge detection in power cables via time-domain convolutional neural networks," *J. Elect. Eng. Technol.*, vol. 14, pp. 1299–1309, 2019.

[16] Y. Wang, J. Yan, Z. Yang, T. Liu, Y. Zhao, and J. Li, "Partial discharge pattern recognition of gas-insulated switchgear via a light-scale convolutional neural network," *Energies*, vol. 12, no. 24, 2019, Art. no. 4674.

[17] W. Wang and N. Yu, "Partial discharge detection with convolutional neural networks," in *Proc. Int. Conf. Probabilistic Methods Appl. Power Syst.*, 2020, pp. 1–6.

[18] X. Peng et al., "A convolutional neural network-based deep learning methodology for recognition of partial discharge patterns from high-voltage cables," *IEEE Trans. Power Del.*, vol. 34, no. 4, pp. 1460–1469, Aug. 2019.

[19] E. Gulski and A. Krivda, "Neural networks as a tool for recognition of partial discharges," *IEEE Trans. Elect. Insul.*, vol. 28, no. 6, pp. 984–1001, Dec. 1993.

[20] B. Adam and S. Tenbohlen, "Classification of multiple PD sources by signal features and LSTM networks," in *Proc. IEEE Int. Conf. High Voltage Eng. Application*, 2018, pp. 1–4.

[21] S. Adavanne, A. Politis, J. Nikunen, and T. Virtanen, "Sound event localization and detection of overlapping sources using convolutional recurrent neural networks," *IEEE J. Sel. Topics Signal Process.*, vol. 13, no. 1, pp. 34–48, Mar. 2019.

[22] C. P. Beura, P. Wenger, E. Tozan, M. Beltle, and S. Tenbohlen, "Classification of partial discharge sources in HVDC gas insulated switchgear using neural networks," in *Proc. VDE High Voltage Technol. 4. ETG- Symp.*, 2022, pp. 1–6.

[23] G. Li, X. Wang, X. Li, A. Yang, and M. Rong, "Partial discharge recognition with a multi-resolution convolutional neural network," *Sensors*, vol. 18, no. 10, 2018, Art. no. 3512.

[24] A. Tröger, U. Riechert, S. Burow, and S. Tenbohlen, "Sensitivity evaluation of different types of PD sensors for UHF-PD-measurements," in *Proc. Int. Conf. Condition Monit. Diagnosis*, 2010. [Online]. Available: https://www.ieh.uni-stuttgart.de/dokumente/publikationen/2010_CMD_Burow_Sensitivity_Evaluation_of_Different_Types_of_PD.pdf

[25] S. Seitz, J. Müller, R. Tetzlaff, and P. Holstein, "Neural networks for the classification of electrical discharges," in *Advances in Acoustics*. Berlin, Germany: German Acoustical Society, 2017, pp. 1019–1021.

[26] S. Mieruch, S. Demirel, S. Simoncelli, R. Schlitzer, and S. Seitz, "SalaciaML: A deep learning approach for supporting ocean data quality control," *Front. Mar. Sci.*, vol. 8, 2021, Art. no. 611742.

[27] D. P. Kingma and J. Ba, "Adam: A method for stochastic optimization," in *Proc. Int. Conf. Learn. Representations*, San Diego, CA, USA, 2015.

[28] G. Li, X. Wang, X. Li, A. Yang, and M. Rong, "Partial discharge recognition with a multi-resolution convolutional neural network," *Sensors*, vol. 18, no. 10, 2018, Art. no. 3512.

[29] G. Behrmann and J. Smajic, "RF PD signal propagation in GIS: Comparing S-parameter measurements with an RF transmission model for a short section of GIS," *IEEE Trans. Dielectrics Elect. Insul.*, vol. 23, no. 3, pp. 1331–1337, Jun. 2016.

Steffen Seitz received the Diploma (Dipl.-Ing.) degree in electrical engineering from the Technische Universität Dresden, Dresden, Germany, in 2016. He is currently advancing his academic career as a Ph.D. candidate and Research Associate with the Chair of Fundamentals of Electrical Engineering, under the guidance of Ronald Tetzlaff. His research interests include neural network-based condition monitoring and explainable artificial intelligence, with a specific focus on enhancing the understandability of model reasoning in predictive maintenance.

Thomas Götz received the Diploma in electrical engineering and the Ph.D. degree in high voltage engineering from the Technische Universität Dresden, Dresden, Germany, in 2015 and 2022, respectively. From 2015 to 2022, he was a Research Associate with the Chair of High Voltage and High Current Engineering, where he headed the Research Group High Voltage Engineering, between 2022 and 2023. He is a member of the CIGRE WG D1.63 Partial discharge detection under DC voltage stress. One of his journal publications was the recipient of the National Literature Award.

Christopher Lindenberg is currently working toward the B.Sc. degree in computer science together with Steffen Seitz and Ronald Tetzlaff with the Technische Universität Dresden, Dresden, Germany. His current research interests include neural network-based failure diagnosis and condition monitoring at the Chair of Fundamentals of Electrical Engineering.

Ronald Tetzlaff (Senior Member, IEEE) is currently the Head of the Chair of Fundamentals of Electrical Engineering, Technische Universität Dresden, Dresden, Germany. Since 2020, he has been the Chief Officer of Technology Transfer and Internationalization with the Technische Universität Dresden. His scientific interests include problems in signal and system theory, medical signal processing, stochastic processes, system modeling, system identification, machine learning, mem-elements, memristive systems, volterra systems, physical fluctuation phenomena, and cellular nonlinear networks.

Stephan Schlegel received the Doctoral and the Habilitation degrees in electrical engineering from the Technische Universität Dresden (TU Dresden), Dresden, Germany, in 2011 and 2019. He led the Research Group Electrical Contacts and Connection between 2011 and 2020. Since 2020, he has been a provisional holder of the Chair of High Voltage and High Current Engineering, the TU Dresden. His research interests include fundamentals of the electrical-mechanical-thermal contact behavior as well as the aging mechanisms and long-term behavior of electrical contacts and connections.